


The secondary-structured DNA-binding activity of Dna2 endonuclease/helicase is critical to cell growth under replication stress

Soyeong Park, Nargis Karatayeva, Annie Albert Demin, Palinda Ruvan Munashingha and Yeon-Soo Seo 

Department of Biological Sciences, Korea Advanced Institute of Science and Technology, Daejeon, Korea

Keywords

checkpoint control; DNA replication; DNA secondary structure; Dna2; DNA-binding protein

Correspondence

Y.-S. Seo, Department of Biological Sciences, Korea Advanced Institute of Science and Technology, Daejeon 34141, Korea.

Tel: +82 42 350 2637

Email: yeonsooseo@kaist.ac.kr

(Received 5 April 2020, revised 11 June 2020, accepted 30 June 2020)

doi:10.1111/febs.15475

Dna2 can efficiently process 5' flaps containing DNA secondary structure using coordinated action of the three biochemical activities: the N-terminally encoded DNA-binding activity and the C-terminally encoded endonuclease and helicase activities. In this study, we investigated the cross talk among the three functional domains using a variety of *dna2* mutant alleles and enzymes derived thereof. We found that disruption of the catalytic activities of Dna2 activated Dna2-dependent checkpoint, residing in the N-terminal domain. This checkpoint activity contributed to growth defects of *dna2* catalytic mutants, revealing the presence of an intramolecular functional cross talk in Dna2. The N-terminal domain of Dna2 bound specifically to substrates that mimic DNA replication fork intermediates, including Holliday junctions. Using site-directed mutagenesis of the N-terminal domain of Dna2, we discovered that five consecutive basic amino acid residues were essential for the ability of Dna2 to bind hairpin DNA *in vitro*. Mutant cells expressing the *dna2* allele containing all five basic residues substituted with alanine displayed three distinct phenotypes: (i) temperature-sensitive growth defects, (ii) bypass of S-phase arrest, and (iii) increased sensitivity to DNA-damaging agents. Taken together, our results indicate that the interplay between the N-terminal regulatory and C-terminal catalytic domains of Dna2 plays an important role *in vivo*, especially when cells are placed under replication stress.

Introduction

DNA repeats pose a great challenge to DNA replication machineries, and their instability is the underlying cause of more than thirty human hereditary diseases [1–3]. Disease-causing repetitive sequences are predisposed to instability, especially when they are converted into long single-stranded DNA (ssDNA) during lagging-strand DNA replication [1,4–7]. For example, the RNA/DNA primer in the downstream Okazaki

fragment can be converted into a single-stranded 5' flap structure by the displacement synthesis activity of DNA polymerase δ , which extends the upstream Okazaki fragment [8,9]. When 5' flaps are short (<6 nt), they are most likely processed by the structure-specific nuclease, Rad27 (FEN1 in humans), generating ligatable nicks [10,11]. With diminished Rad27 activity, the 5' flaps can grow longer, increasing the possibility of

Abbreviations

5-FOA, 5-fluoroorotic acid; aa, amino acids; CPT, camptothecin; CV, column volume; ds, double-stranded; DSB, double-strand break; EMSA, electrophoretic mobility shift assay; GST, glutathione S-transferase; His₆, hexahistidine; HJ, Holliday junction; IDZ, imidazole; IPTG, isopropyl β -D-1-thiogalactopyranoside; LC-MS/MS, liquid chromatography/tandem mass spectrometry; MMS, methyl methanesulfonate; Ni-NTA, Ni²⁺-nitrilotriacetic acid; NTD, N-terminal DNA-binding domain; RPA, replication protein A; SDS/PAGE, sodium dodecyl sulfate/polyacrylamide gel electrophoresis; ss, single-stranded; ssc, single-stranded circular; YPD, yeast extract/peptone/dextrose.

forming flaps with secondary-structured DNA, including hairpins; these flaps would be more prominent, especially when they contain structure-forming repetitive sequences [12–15]. Moreover, it has been shown that the nuclease activity of Rad27 is inhibited in cases where flaps contain secondary structure or are coated with replication protein A (RPA), a eukaryotic single-stranded DNA-binding protein [15–17].

In contrast to Rad27, Dna2 is an endonuclease/helicase that plays a critical role in removing long flaps, particularly secondary-structured or RPA-coated 5' flaps, during lagging strand maturation [16,18,19]. The N-terminal DNA-binding domain (amino acids 1–405) of Dna2 harbors a structure-specific DNA-binding activity toward 5' flaps containing a hairpin structure [18]. It has been shown that the N-terminal DNA-binding activity and the C-terminal catalytic activities of Dna2 are coupled so as to resolve and remove secondary-structured 5' flaps that have escaped cleavage by Rad27 [16,18,20]. In fact, it was reported that DNA sequence containing 174 repeats of CTG nucleotides, which can form secondary structures, is less stable in the cells harboring mutant Dna2 devoid of the N-terminal DNA-binding domain [18]. However, the structural requirement of 5' flaps with respect to binding the N-terminal domain of Dna2 and the *in vivo* significance of this binding activity have not been fully investigated.

In addition to secondary-structured DNA-binding activity, the N-terminal domain of Dna2 possesses two other important functions that could contribute to genome stability. Cdk1-dependent phosphorylation of T4, S17, and S237 residues of Dna2 facilitates the recruitment of Dna2 to double-strand break (DSB) repair sites [21,22]. Also, W128 and Y130 residues are required for stimulation of the checkpoint kinase Mec1 and subsequent activation of the S-phase checkpoint under conditions of replication stress [23]. This checkpoint-initiation activity indicates that Dna2, through its N-terminal domain, serves as a checkpoint sensor [24,25]. Therefore, it appears that the N-terminal domain of Dna2 has a regulatory role in promoting the repair of aberrant DNA intermediates in addition to guiding Dna2 to secondary-structured flaps for removal. However, functional interactions between these regulatory activities and the previously identified catalytic activities of Dna2 are currently not well-understood.

In this study, we examined the physiological significance and interplay of the regulatory and catalytic activities of Dna2 in *Saccharomyces cerevisiae*. We found that the disruption of the catalytic activities of Dna2 activated Dna2-dependent checkpoint. The N-terminal domain of Dna2 bound specifically to

substrates that mimic DNA replication fork intermediates, including Holliday junctions. We also mapped amino acid residues in the N-terminal domain of Dna2 important for its function in this regard. Our results emphasize the importance of the N-terminal DNA-binding domain of Dna2 for normal cell growth as well as under replication stress.

Results

Dna2-induced Mec1 activation causes growth defects in *dna2* catalytic mutant cells

Yeast cells harboring nuclease- or helicase-deficient *dna2* alleles exhibit growth defects [26–30]. These growth defects can be partially overcome by mutations of checkpoint genes [8,28,29,31–33]. Interestingly, Dna2 is able to activate checkpoint through its W128 and Y130 residues by stimulating Mec1 (a yeast ortholog of human ATR), the apical checkpoint kinase [23]. Alanine substitution of W128 and Y130 (*dna2-WY-AA* mutation, Fig. 1A) abrogates the Mec1-stimulatory activity of Dna2 [23]. This raises the possibility that the elimination of the Dna2-dependent checkpoint could suppress growth defects in *dna2* catalytic mutant cells.

To test this possibility, we combined the *dna2-WY-AA* mutation with various enzyme activity-defective *dna2* mutant alleles, including *dna2-K1080E* (*dna2-KE*, helicase-deficient), *dna2-H547A* (*dna2-HA*, nuclease-attenuated), and *dna2-D657A* (*dna2-DA*, nuclease-deficient) (Fig. 1A) [26,30]. The mutation in the *dna2-KE* allele abrogates ATP-binding activity of the protein, thereby inactivating its helicase activity, and becomes lethal to cells when present in a low-copy plasmid [20,26,30]. Yeast cells harboring the *dna2-HA* allele display partial growth defects owing to the reduced nuclease activity of Dna2 (~50% of wild-type), whereas the *dna2-DA* allele completely abrogates the nuclease activity and is lethal [30].

To examine the phenotypes of various *dna2* mutant alleles newly constructed, we deleted genomic wild-type *DNA2* in yeast cells, while maintaining viability by introducing pRS316-*DNA2* plasmid, which contains *URA3* gene as a selection marker [34]. The yeast strain thus prepared was then transformed with pRS314 plasmids expressing the *dna2* mutant genes and *TRP1* gene as a selection marker. Incubation of the transformed cells in the presence of 5-fluoroorotic acid (5-FOA) allowed only those cells that have lost the pRS316-*DNA2* plasmid to survive owing to the toxicity of *URA3*. Using this plasmid shuffling method, we compared the growths of the cells having *dna2-WY-AA*

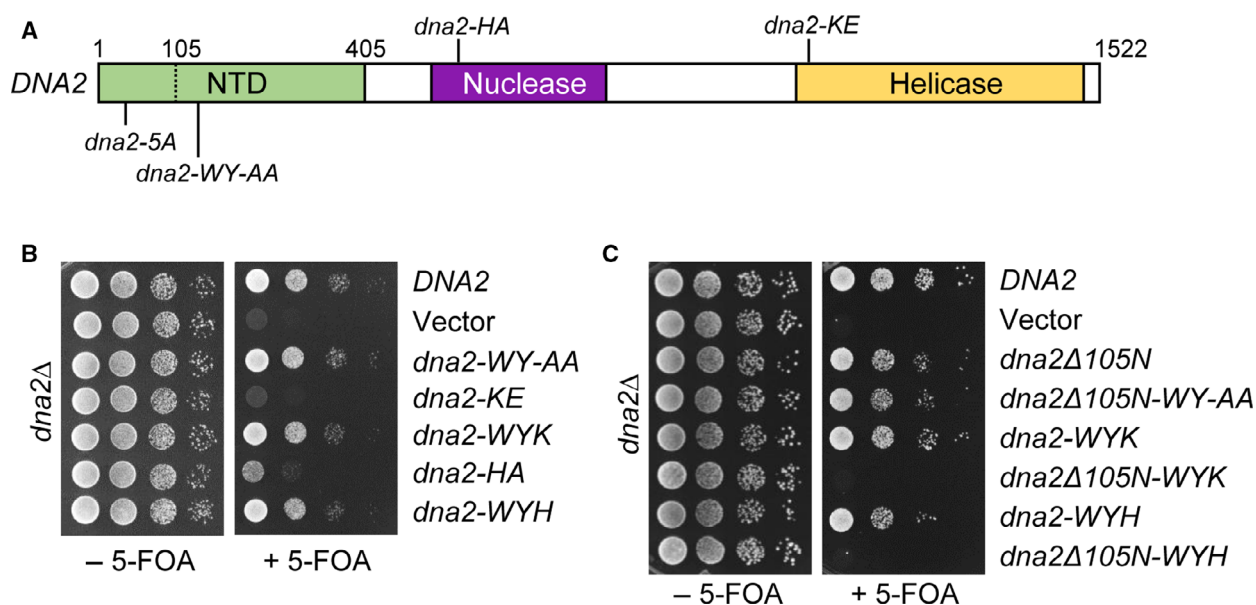


Fig. 1. The *dna2-WY-AA* mutation suppresses the growth defects of *dna2-KE* and *dna2-HA* cells, a suppression that requires the N-terminal 105-amino acid region of Dna2. **A**, Schematic representation of the functional domains of Dna2. Amino acid positions are indicated by numbers. The mutation alleles introduced into the catalytic domains and the N-terminal DNA-binding domain (NTD) are depicted above and below, respectively. *dna2-5A* denotes multiple-point mutations of K41A, R42A, K43A, K44A, and K45A. *dna2-WY-AA*, *dna2-HA*, and *dna2-KE* indicate W128A Y130A double mutation, H547A, and K1080E mutations, respectively. **B** and **C**, YJA1B cells were transformed with pRS314 plasmids harboring the indicated *DNA2* alleles. The drop dilution assays were performed as described in Materials and Methods. Serially diluted mutant yeast cells were then spotted onto synthetic dropout media lacking or containing 5-fluoroorotic acid (5-FOA) and incubated at 30 °C for 2–3 d. The presence of 5-FOA forces elimination of pRS316-*DNA2*, allowing the phenotypes of mutant *dna2* alleles to penetrate. The drop dilution experiments were repeated three times, and one representative result was shown.

mutation in combination with the various *dna2* catalytic mutant alleles as shown in Figs. 1B,C.

Cells harboring wild-type *DNA2* gene (positive control) in plasmid were able to support robust growth in the presence of 5-FOA, whereas cells transformed with an empty vector (negative control) could not grow under the same conditions (Fig. 1B). This agrees with the previous finding that Dna2 is essential for cell growth [27]. In addition, the *dna2-WY-AA* cells showed no noticeable growth defects by itself, as previously demonstrated [23], whereas both *dna2-KE* and *dna2-HA* cells exhibited severe growth defects (Fig. 1B). However, we found that *dna2-WY-AA* mutation efficiently suppressed the defective growth phenotype of *dna2* catalytic mutants since cells harboring combined mutations of *dna2-WY-AA* with *dna2-KE* or *dna2-HA* (*dna2-WYK* and *dna2-WYH*, respectively) grew as efficiently as cells with wild-type *DNA2* (Fig. 1B, compare *dna2-WYK* and *dna2-WYH* with *DNA2*). We found that the lethality of nuclease-dead mutant (*dna2-DA*) cells could not be rescued by the *dna2-WY-AA* mutation (data not shown), which agrees with the finding that Dna2 nuclease activity is most important for cell viability [30]. Collectively, these

results suggest that the growth defects of *dna2-KE* and *dna2-HA* cells could be attributed to Dna2-mediated stimulation (via W128 and Y130 residues) of the Mec1-dependent checkpoint (Fig. 1B). We were not able to confirm this unambiguously since *dna2-KE* and *dna2-HA* mutants are lethal or close to lethal, respectively, in the absence of a wild-type copy of *DNA2*. This has hindered a rigorous analysis of *dna2-KE* and *dna2-HA* mutants. It should be noted that this result above does not exclude the possibility that Dna2-independent checkpoint is activated in the *dna2-WYK* and *dna2-WYH* mutants to repair the lesions, as evidenced by the robust growth of these cells.

The N-terminal 105-amino acid region is essential for *dna2-WYK* and *dna2-WYH* cells

Yeast cells harboring a *dna2* allele in which the N-terminal 105 amino acids (aa) are deleted exhibit temperature-sensitive growth [35]. This implies that the first 105-aa region of Dna2 contributes critically to its optimal functioning *in vivo*. To examine the precise role of the N-terminal 105 aa in this regard, we truncated this region of the N-terminal domain in *dna2-WYK* and

dna2-WYH and examined their viability similarly as described above. We observed that deletion of 105 aa from the N terminus of both *DNA2* and *dna2-WY-AA* alleles had no significant effect on cell growth at 30 °C (Fig. 1C) [35]. In contrast, 105-aa truncation of the *dna2-WYK* (*dna2Δ105N-WYK*) and *dna2-WYH* alleles (*dna2Δ105N-WYH*) completely abolished cell growth (Fig. 1C). These results suggest that the N-terminal 105-aa region plays a critical function for cell viability when the catalytic activity of Dna2 is defective.

It was reported that Cdk1-dependent phosphorylation of T4, S17, and S237 residues in the N-terminal domain of Dna2 is important for recruitment of Dna2 to DSB repair sites [21]. Substitution of alanine for T4, S17, and S237 (*dna2-3A* mutation) was shown to reduce the efficiency of DSB resection [21]. Therefore, it is possible that the viability of *dna2Δ105N-WYK* and *dna2Δ105N-WYH* cells is lost because of the loss of T4 and S17 residues that participate in DSB recruitment. To test this possibility, we combined *dna2-3A* mutation with the *dna2-KE* allele and found that *dna2-3A* partially suppressed the growth defect of *dna2-KE* cells (data not shown). This indicates that loss of T4 and S17 residues is not likely to be the direct cause of lethality in *dna2Δ105N-WYK* cells.

Structural requirements of DNA substrates for binding the N-terminal domain of Dna2

Previous reports have shown that efficient removal of secondary-structured flaps during Okazaki fragment processing requires the coordinated action of the N-terminal DNA binding, endonuclease, and helicase activities of Dna2 [18,20]. Therefore, it is possible that loss of the coordinated activities of the N-terminal DNA binding and catalytic activities may have induced the lethality of *dna2Δ105N-WYK* and *dna2Δ105N-WYH* cells. This led us to examine the structural requirements of DNA substrate for binding Dna2 and to map the precise location of the N-terminal DNA-binding activity of Dna2.

To this end, a truncated, N-terminally FLAG-tagged and hexahistidine (His₆)-tagged recombinant protein comprising the first 405 aa of Dna2 (Dna2^{405N}) was expressed and purified from *E. coli*. To verify that the DNA-binding activity was intrinsic to Dna2^{405N}, we collected the peak fraction of Dna2^{405N} from the final Ni²⁺-NTA column chromatography and separated it by glycerol gradient sedimentation. Each glycerol gradient fraction was analyzed for protein content and then assayed for DNA-binding activity by electrophoretic mobility shift assay (EMSA) using the

standard 5' hairpin flap DNA as a substrate. We found that the amount of DNA substrate bound was proportional to the amount of protein present in the glycerol gradient fraction (data not shown). These results confirm that the previously identified hairpin DNA-binding activity is intrinsic to the purified Dna2^{405N} protein [18].

Next, we compared the DNA-binding activity of Dna2^{405N} using three different flap substrates; these contained 48-nt oligo-dT (dT), 16 repeats of CTG (CTG), or 15-nt ssDNA + 15-bp hairpin (Hairpin) in the flap, as illustrated in Fig. 2A. In the absence of competitor DNA, Dna2^{405N} formed nucleoprotein complexes with all three substrates with varying efficiencies, under the reaction condition tested. The Hairpin substrate was the most efficient, followed in order by CTG and dT substrates in the absence of competitor DNA (Fig. 2A, – competitor). In the presence of a 15-fold excess of poly(dI-dC), a nonspecific double-stranded DNA (dsDNA) competitor, Dna2^{405N} failed to show any detectable binding activity to the dT substrate. In contrast, Dna2^{405N} were still able to bind CTG and Hairpin substrates, both containing secondary structures (Fig. 2A, + competitor).

To reinforce the finding that secondary-structured flap DNA is a preferred binding substrate of Dna2^{405N}, we tested the effects of two other types of competitor DNA: synthetic 50-nt poly dT and M13mp18 viral DNA. The synthetic 50-nt poly dT is a ssDNA that is expected to be devoid of any secondary structure, whereas native M13mp18 viral DNA is a long ss circular DNA (sscDNA) with extensive secondary structure in solution [36].

Dna2^{405N} was incubated with Hairpin substrate and the indicated amount of competitor DNA under the standard EMSA condition. As expected, the addition of synthetic 50-nt poly dT (ssDNA) to the reaction mixtures barely inhibited the formation of nucleoprotein complex, even at the highest concentration (40 ng; 60-fold excess) used (Fig. 2B). Poly(dI-dC) (dsDNA) showed a moderate level of competition (~40% inhibition with 5 ng; sevenfold excess). In contrast, M13mp18 viral DNA (sscDNA) was an effective competitor, markedly reducing (>80%) the amount of nucleoprotein complexes when added in sevenfold excess. These results confirm that DNA containing a high level of secondary structure can efficiently compete with 5' hairpin flap substrates for Dna2^{405N} binding, and provide strong evidence that the N-terminal domain of Dna2 preferentially binds secondary-structured DNA.

We then examined the binding affinities of Dna2^{405N} to various types of hairpin flap substrates that could

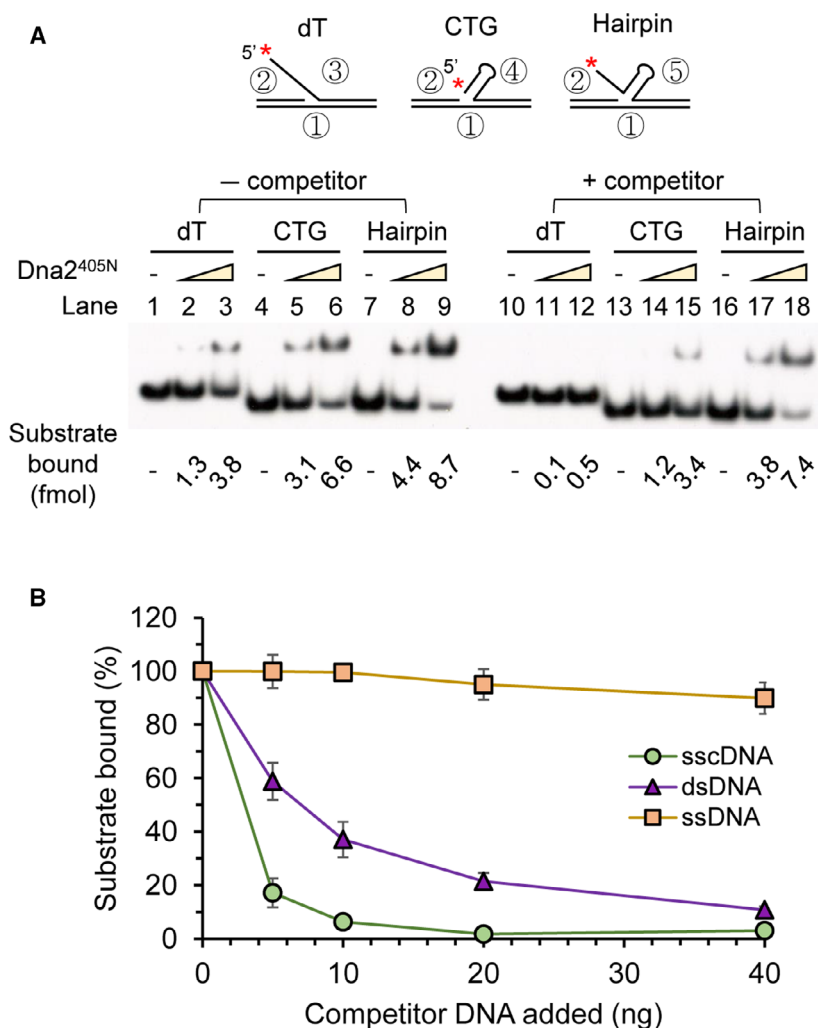


Fig. 2. Purified recombinant Dna2^{405N} protein prefers to bind secondary-structured DNA over unstructured ones. *A*, Electrophoretic mobility shift assay (EMSA) was conducted using 1 and 2 ng of Dna2^{405N} in the absence of the competitor, poly(dI-dC), and 2 and 5 ng in the presence of the competitor. The asterisk indicates the position of ³²P label. The EMSA experiments were repeated more than five times, and one representative result was shown. *B*, Dna2^{405N} (2 ng) was incubated with 15 fmol of the Hairpin substrate in the presence of the indicated amounts of competitors and analyzed by EMSA. Single-stranded (ss) DNA, double-stranded (ds) DNA, and single-stranded circular (ssc) DNA denote 50-nt-long oligo-dT, poly(dI-dC), and M13mp18 viral DNA, respectively. Error bars denote standard deviation from three independent experiments

arise during Okazaki fragment processing. First, we tested flap substrates with varying lengths (0–15 nt) between the hairpin and the duplex template DNA, as depicted in Fig. 3A. We found that the binding activity of Dna2^{405N} was, in general, inversely proportional to the distance between the hairpin and the duplex template DNA (Fig. 3A); the longer the ssDNA linker was, the lower the amount of protein–DNA complex formed. The presence of 2-nt and 5-nt ssDNA linkers resulted in ~20% and ~50% reductions in the amount of complex formed, respectively, compared with the substrate that does not have a linker. The substrate containing a 15-nt ssDNA linker bound poorly to Dna2^{405N}. Therefore, these results suggest that the N-terminal domain of Dna2 preferentially binds to the three-way arm structure of a flap substrate, which resembles freshly generated hairpin flaps during Okazaki fragment processing.

Dna2^{405N} showed a moderate level of binding to the CTG substrate compared with the Hairpin substrate

(Fig. 2A). The apparent structural difference between them is the presence of a 5' single-strand tail in the Hairpin substrate. This prompted us to investigate the influence of a 5' ssDNA tail on Dna2^{405N} binding. To this end, we compared binding activities of Dna2^{405N} among the hairpin flap substrates possessing 5' ss tails of varying lengths (Fig. 3B). The substrate containing a 5-nt tail was less efficient (~50%) in binding Dna2^{405N} than was the substrate with a 15-nt tail. The flap substrate completely lacking a 5' ssDNA tail segment exhibited a significant reduction (>80%) in binding. Therefore, the 5' ss tail structure acts as an important element for Dna2 binding. This observation is consistent with the preferred substrate structures for the nuclease and helicase activities of Dna2 [18–20,37,38].

To examine the binding affinity of Dna2^{405N} to DNA replication intermediates other than flap structures, we prepared DNA substrates that mimic regular and partially regressed leading and lagging strand replication forks, as illustrated in Fig. 3C. The regular

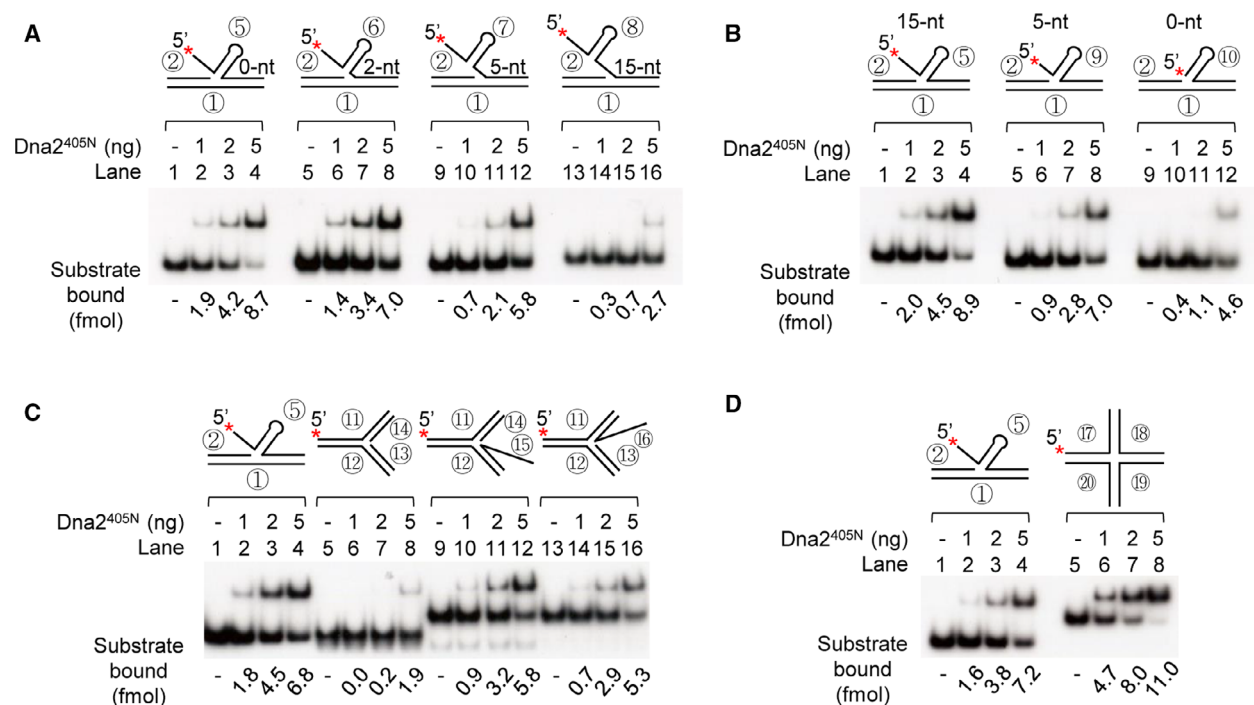


Fig. 3. Dna2^{405N} exhibits robust binding affinity to various replication intermediates. Standard EMSAs were conducted using the indicated amounts of Dna2^{405N} and substrates. The EMSA experiments were repeated three times, and one representative result was shown. *A* and *B*, Hairpin flap DNA substrates with varying linker (*A*) and 5' ssDNA tail (*B*) lengths were used as substrates. *C* and *D*, DNA substrates mimicking replication fork intermediates (*C*) and Holliday junction structure (*D*) were used as substrates

replication fork-like DNA substrate was a poor substrate for Dna2^{405N} binding (lanes 5–8). In contrast, both partially regressed lagging strand (lanes 9–12) and leading strand (lanes 13–16) replication fork structures were active in Dna2^{405N} binding, displaying 60–80% of the binding efficiency to the standard Hairpin substrate (Fig. 3C). We also tested Holliday junction (HJ) DNA, a four-way arm that mimics the regressed ‘chicken-foot’ structure of replication forks. We found that this substrate was nearly twice as active as the standard hairpin substrate in Dna2^{405N} binding (Fig. 3D). Thus, the N-terminal domain of Dna2 possesses specific binding activity for two types of partially regressed replication fork intermediates and HJ structure. The significance of robust binding of Dna2 to these structures is not clear, but will be discussed below.

Mapping hairpin-flap-binding activity within the N-terminal domain of Dna2

To map the critical region carrying the hairpin-flap-binding activity, we created N-terminal domain truncation mutants of Dna2, as depicted in Fig. 4A. All derivatives possessed GST and His₆ tags fused to the N

terminus and C terminus, respectively, to facilitate purification and detection of nucleoprotein complexes during gel analyses. The truncated forms of the N-terminal domain were purified using two affinity-column chromatographic steps as described in Materials and Methods (Fig. 4B). We found that DNA-binding activities of Dna2^{405N} and GST-Dna2^{405N}-His₆ were indistinguishable (data not shown). This indicates that the presence of GST and His₆ tags in the proteins did not interfere with the DNA-binding activity. Further test of hairpin-flap-binding activities of purified proteins showed that GST-Dna2^(1–202)-His₆ retained DNA-binding activity comparable to that of GST-Dna2^{405N}-His₆, whereas GST-Dna2^(1–100)-His₆ was ~50% as active as GST-Dna2^{405N}-His₆ (Fig. 4C). In contrast, both GST-Dna2^(101–405)-His₆ and GST-Dna2^(203–405)-His₆ binding could not be detected. Therefore, it appears that the first 100-aa segment of the N-terminal domain contains the critical region for binding hairpin flap DNA. The second 100-aa region (aa 101–202) may play an auxiliary role, possibly providing stability of the nucleoprotein complex after the initial binding event takes place by the first 100-aa region. This is in keeping with the observation that GST-Dna2^(101–405)-His₆ could not bind the hairpin flap DNA substrate.

Previous studies have shown that the N-terminal domain of Dna2 is prone to nonspecific proteolysis, suggesting that the domain is intrinsically unstructured [18,35]. Consistent with this, DNA-binding activity of Dna2^{405N} was retained after heat treatment of the protein (data not shown), a feature often associated with unstructured proteins [39]. Therefore, it seems reasonable to assume that the purified recombinant Dna2^{405N} is also unstructured. In addition, it is well accepted that intrinsically unstructured proteins often undergo a conformational transition from an unstructured state to a structured state upon binding to their physiological interaction partner [39]. Since substrate-induced

folding may produce a local globular structure that confers resistance to proteolytic digestion, we investigated whether the N-terminal domain of Dna2 forms a rigid structure when bound to DNA substrates. To this end, we subjected Dna2^{405N} to proteolysis by subtilisin, a nonspecific protease, in the presence of blunt-ended dsDNA (pUC19 plasmid digested with DpnI) or sscDNA (M13mp18 viral DNA).

In the absence of DNA, Dna2^{405N} was highly sensitive to subtilisin and was completely digested by 10 ng of subtilisin (Fig. 4D, lane 4). The presence of dsDNA in the binding reaction yielded a digestion pattern similar to that obtained in the reaction without DNA

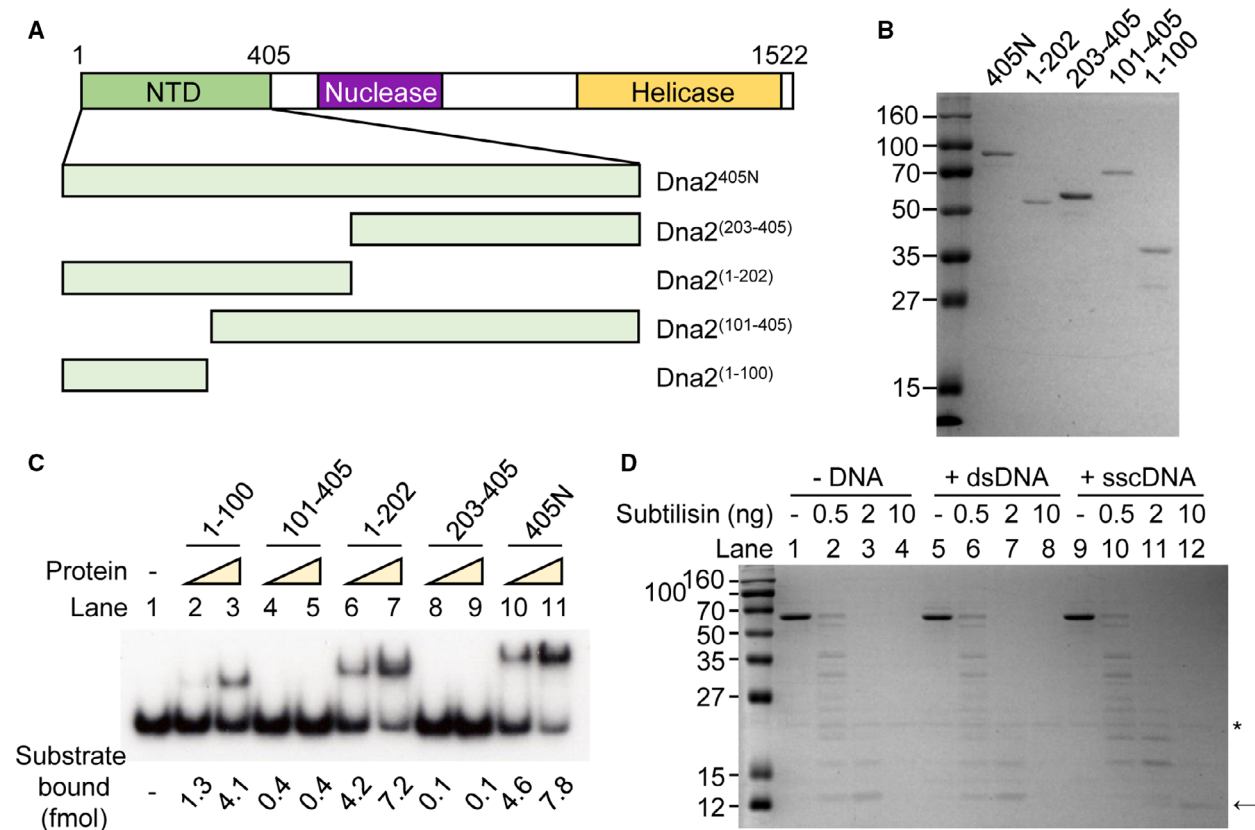


Fig. 4. The N-terminal 1- to 125-amino acid region harbors the hairpin-flap-binding activity of Dna2. *A*, Schematic illustrations of Dna2 domain structure (top) and truncated forms of N-terminal segment (bottom). *B*, Each protein fragment in panel *A* was tagged with glutathione S-transferase (GST) and hexahistidine (His₆) at N terminus and C terminus, respectively. The purified GST-Dna2^{405N}-His₆, GST-Dna2⁽¹⁻²⁰²⁾-His₆, GST-Dna2⁽²⁰³⁻⁴⁰⁵⁾-His₆, GST-Dna2⁽¹⁰¹⁻⁴⁰⁵⁾-His₆, and GST-Dna2⁽¹⁻¹⁰⁰⁾-His₆ (denoted as 405N, 1-202, 203-405, 101-405, and 1-100, respectively) were separated by sodium dodecyl sulfate/polyacrylamide gel electrophoresis (SDS/PAGE) on 12% gels and stained with Coomassie Brilliant Blue. The numbers on the left side represent protein marker sizes (in kDa). One representative result of SDS/PAGE was shown. *C*, Increasing amounts (50 and 100 fmol) of each protein in panel *A* were incubated with 15 fmol of the standard 5' hairpin flap substrate and analyzed by EMSA. The EMSA experiments were repeated three times, and one representative result was shown. *D*, Dna2^{405N} (1 μg) was incubated without DNA (lanes 1-4) or with dsDNA (DpnI-digested pUC19, lanes 5-8) or sscDNA (M13mp18, lanes 9-12), followed by addition of the indicated amounts of subtilisin. The mixtures were then resolved by SDS/PAGE on 15% gels and stained with Coomassie Brilliant Blue. The asterisk indicates a nonspecific band. The subtilisin-resistant protein band is indicated by an arrow. One representative result of SDS/PAGE was shown

(Fig. 4D, compare lanes 1–4 and lanes 5–8). In strong contrast, we found that addition of sscDNA produced a 12-kDa proteolytic fragment from protease-treated Dna2^{405N} (Fig. 4D, lane 12, indicated with an arrow). This fragment was highly resistant to proteolysis, as evidenced by its ability to survive treatment up to 50 ng of subtilisin (data not shown). This level of proteolytic resistance is comparable to that of BSA, which has a well-defined rigid structure [40]. This result confirms that the region of Dna2^{405N} corresponding to the 12-kDa proteolytic fragment is converted into a defined structure when bound to DNA substrate.

To determine the protease-resistant region within Dna2^{405N}, we excised the band containing the subtilisin-resistant fragment from the SDS/PAGE gel, treated it with trypsin, and then subjected it to liquid chromatography/tandem mass spectrometry (LC-MS/MS). Mass-to-charge scores from MS and MS/MS data identified N- and C-terminal peptide sequences that correspond to the 13- to 125-aa fragment of Dna2 (data not shown). This result is consistent with our finding that the first 100-aa fragment is important for the hairpin-flap-binding activity.

A group of five positively charged amino acids in the N-terminal domain of Dna2 is essential for hairpin-flap-binding activity

Next, we sought to determine whether the N-terminal domain of Dna2 has locally stable secondary structures such as α -helices. To this end, we analyzed the propensity of the N-terminal domain of Dna2 to adopt such structures using the bioinformatic tool, IUPred2A Web server. This tool predicts intrinsically disordered region (s) within a protein by calculating disorder scores at the amino acid level [41]. Disorder score values range from 0 to 1; regions where values are less than 0.5 are considered to be structured [42]. Sequence analysis of the N-terminal 405-aa domain of Dna2 using IUPred2A revealed that the entire region is highly disordered, with several positions exhibiting drops in value close to or slightly below 0.5 (Fig. 5A, bottom). Focusing on the N-terminal 125-aa segment, to which the hairpin DNA-binding activity was mapped, we found that residue K44 had the lowest disorder score of 0.47 (Fig. 5A, top). This residue belongs to a basic residue cluster that consists of five positively charged amino acid residues (K41, R42, K43, K44, and K45). This cluster occurs only once in the N-terminal 125-aa region of Dna2.

To investigate whether the positively charged cluster contributes to the hairpin-flap-binding activity of Dna2^{405N}, we prepared a recombinant GST-Dna2^{405N}-5A-His₆ protein in which all five basic amino acids

(K41–K45) were mutated to alanine (*dna2-5A* mutation, Fig. 1A and 5B) and tested for hairpin-flap-binding activity. We observed that wild-type (WT) GST-Dna2^{405N}-His₆ protein efficiently bound Hairpin substrate. However, GST-Dna2^{405N}-5A-His₆ (5A) protein did not show any detectable binding activity to the same substrate (Figs. 5C,D). The result was reproducible when we used full-length Dna2 and Dna2-5A proteins purified from insect cells using a baculoviral expression system (data not shown). Taken together, these observations suggest that the basic K41–K45 patch in the N-terminal domain of Dna2 is essential in binding hairpin flap DNA.

Cell cycle is arrested at late S or G2/M phase in *dna2-5A* cells at 37 °C

To examine the physiological significance of the *dna2-5A* mutation and, hence, the hairpin-binding activity of Dna2, we constructed a mutant strain expressing *dna2-5A* in place of wild-type *DNA2* gene. The *dna2-5A* cells showed a slow-growth phenotype at elevated temperatures of 34 °C and 37 °C, whereas its growth at 30 °C was comparable to that of wild-type (Fig. 6A). As expected, the temperature sensitivity observed was efficiently suppressed, like *dna2 Δ 405N* lacking the N-terminal 405-aa region, when *RAD27* or *RFA1* (the large subunit of RPA) was overexpressed in a multicopy plasmid (Fig. 6B) [16,43].

We next tested whether bulk DNA synthesis was affected by loss of the hairpin-flap-binding activity of Dna2 at 37 °C. To this end, we assessed the cell cycle progression of *dna2-5A* cells over time by flow cytometric analysis after G1 arrest. Under normal growth conditions (30 °C), WT and *dna2-5A* cells showed comparable cell cycle progression up to 210 min (Fig. 6C, 30 °C). When the cells were incubated at 37 °C, both strains were able to duplicate bulk DNA, as evidenced by the accumulation of cells with 2C DNA content (Fig. 6C, 37 °C). In WT cells, 1C population started to reduce at 90 min, followed by increase at 120 min and thereafter. However, *dna2-5A* cells maintained a high proportion of cells with 2C DNA content from 120 min to 210 min. This indicates that a significant number of *dna2-5A* cells experienced cell cycle arrest at late S or G2/M phase.

To determine whether the observed cell cycle arrest is mediated by checkpoint signaling, we assessed the level of checkpoint activation by monitoring the mobility shift of the endogenous checkpoint kinase Rad53 (Chk2 in humans) on SDS/PAGE gels (Fig. 6D). Rad53 undergoes phosphorylation by Mec1

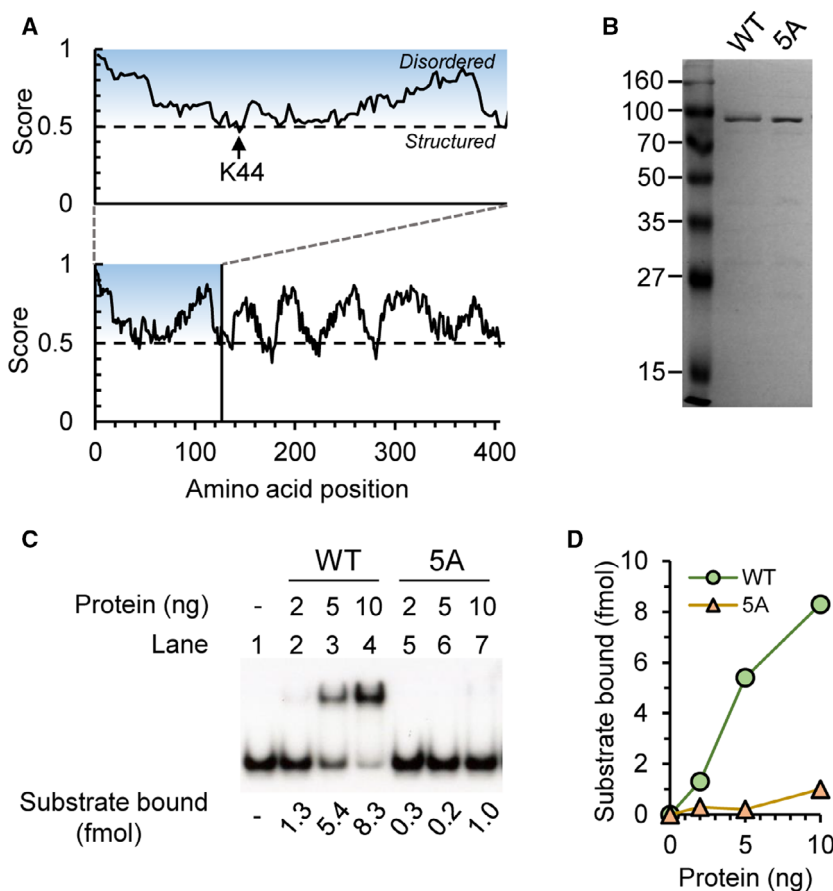


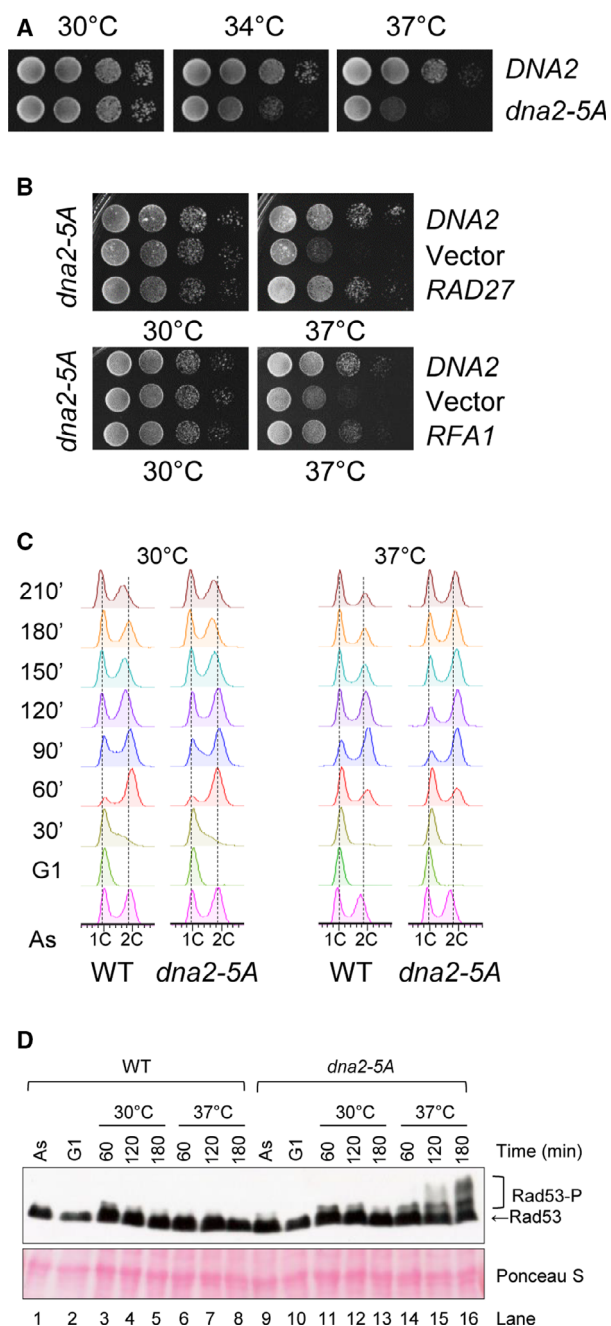
Fig. 5. Point mutation of the five positively charged amino acid residues abolishes the hairpin-flap-binding activity of the N-terminal domain of Dna2. **A**, Graphs show IUPred2A scores of amino acids in the N-terminal domain of Dna2 from amino acids 1 to 125 (top) and 1 to 405 (bottom). Amino acid regions with scores greater than 0.5 are considered to be intrinsically disordered. The lysine 44 (K44) position is indicated by an arrow. **B**, 12% SDS/PAGE gel image of GST-Dna2^{405N}-His₆ (WT) and GST-Dna2^{405N}-5A-His₆ (5A) proteins. One representative result of SDS/PAGE was shown. **C** and **D**, Standard EMSA reactions were conducted using increasing amounts (2, 5, and 10 ng) of WT and 5A proteins, and 15 fmol of the standard 5' hairpin flap substrate (**C**). The EMSA experiments were repeated three times, and one representative result was shown. The result obtained from (**C**) was quantified and graphed in (**D**)

that is activated by Dna2, giving rise to a slowly migrating Rad53 species [23,44]. Cell lysates obtained after release from G1 phase at 30 °C or 37 °C were analyzed by western blotting using a Rad53 antibody. In the case of WT cells, the majority of endogenous Rad53 stayed in an unphosphorylated state at 30 °C and 37 °C (Fig. 6D, lanes 3–8). At 30 °C, results for *dna2-5A* cells were similar to those of WT cells (Fig. 6D, lanes 11–13). However, endogenous Rad53 in *dna2-5A* cells cultured at 37 °C was hyperphosphorylated at 120 and 180 min (Fig. 6D, lanes 15 and 16). These results support the conclusion that the kinase activity of Rad53, and thus Rad53-triggered checkpoint signaling, is activated in *dna2-5A* cells grown at 37 °C. Taken together, these results indicate that loss of the hairpin flap DNA-binding activity of Dna2

induces checkpoint signaling at the restrictive temperature, leading to cell cycle arrest.

Hairpin-flap-binding activity is required for cell growth under replication stress

To elucidate the role of the hairpin-flap-binding activity of Dna2 under replication stress condition, we subjected *dna2-5A* cells to treatment of DNA-damaging agents including methyl methanesulfonate (MMS), an alkylating agent that hinders DNA replication fork progression [45,46] and camptothecin (CPT), which induces DSBs by forming a stable complex with DNA topoisomerase I [47,48]. Unlike wild-type cells, *dna2-5A* mutant cells showed detectable sensitivity to MMS and CPT (Fig. 7A). This result is consistent with the



observations that mutations in the conserved helicase domain of *dna2* displayed sensitivity to MMS and CPT, supporting a functional cross talk between the hairpin flap DNA-binding and helicase activities [29,33]. The sensitivity of *dna2-5A* cells to CPT raises the possibility that the hairpin DNA-binding activity of Dna2 may be important during DSB repair. In this process, extensive ssDNA is generated by the combined action of Sgs1-Top3-Rmi1 during resection of DSBs and the resulting long ssDNA is likely to

Fig. 6. The *dna2-5A* mutation induces defects in growth and cell cycle progression at high temperatures. **A**, Drop dilution assays were performed using wild-type or *dna2-5A* cells on yeast extract/peptone/dextrose (YPD) agar plates at the indicated temperature. The drop dilution experiments were repeated three times, and one representative result was shown. **B**, *dna2-5A* cells were transformed with pRS315-*DNA2* (*DNA2*), pRS325 (Vector), and pRS325 containing either *RAD27* or *RFA1* gene. Drop dilution assays were performed on synthetic dropout media at the indicated temperatures. The drop dilution experiments were repeated three times, and one representative result was shown. **C**, Asynchronous (As) log-phase yeast cells (wild-type (WT) or *dna2-5A*) were arrested at G1 phase by addition of α -factor (G1) and released into fresh YPD media at 30 °C or 37 °C. Samples were withdrawn every 30 min for flow cytometric analysis. The locations of unreplicated and replicated DNA are indicated by 1C and 2C, respectively. **D**, WT and *dna2-5A* cells were grown at 30 °C or 37 °C as described in (C). Cell extracts prepared at each time point were subjected to western blotting with a Rad53 antibody. 'Rad53-P' denotes the phosphorylated forms of Rad53. The western blot experiments were repeated three times, and one representative result was shown

contain hairpins [49]. In fact, we observed that the N-terminal domain of Dna2 possesses robust binding activity to the substrate mimicking resected DNA containing a 5' hairpin (data not shown).

The MMS/CPT-sensitive phenotype was more severe in the *dna2 Δ 405N* strain lacking the entire N-terminal 405-aa domain of Dna2 (Fig. 7A). To further explain the relationship between checkpoint activation and DNA binding, we combined both *dna2-WY-AA* and *dna2-5A* to generate *dna2-5A-WY-AA* and determined whether combination of a DNA binding defect and abrogation of checkpoint activation leads to comparable hypersensitivity of *dna2 Δ 405N* to DNA replication stress. The *dna2-5A-WY-AA* cells showed a nearly comparable sensitivity to a variety of DNA-damaging agents including 4-nitroquinoline 1-oxide, bleomycin, UV, hydroxyurea, MMS, and CPT than *dna2-5A*, but less sensitive than *dna2 Δ 405N* cells (data not shown). This finding is consistent with the previous finding that the N-terminal domain of Dna2 has additional functions, such as recruitment to DSB resection sites [21,23].

The Pif1 helicase was shown to promote the generation of long flaps during Okazaki fragment processing [50–53]. The long flaps formed are likely to contain secondary structures, which require hairpin-binding activity of Dna2 for their removal [18]. Thus, in the absence of a functional copy of *PIF1*, *DNA2* is no longer essential for growth since *pif1* mutants do not produce long flaps. In order to address whether the growth defects of *dna2-5A* and *dna2 Δ 405N* could be

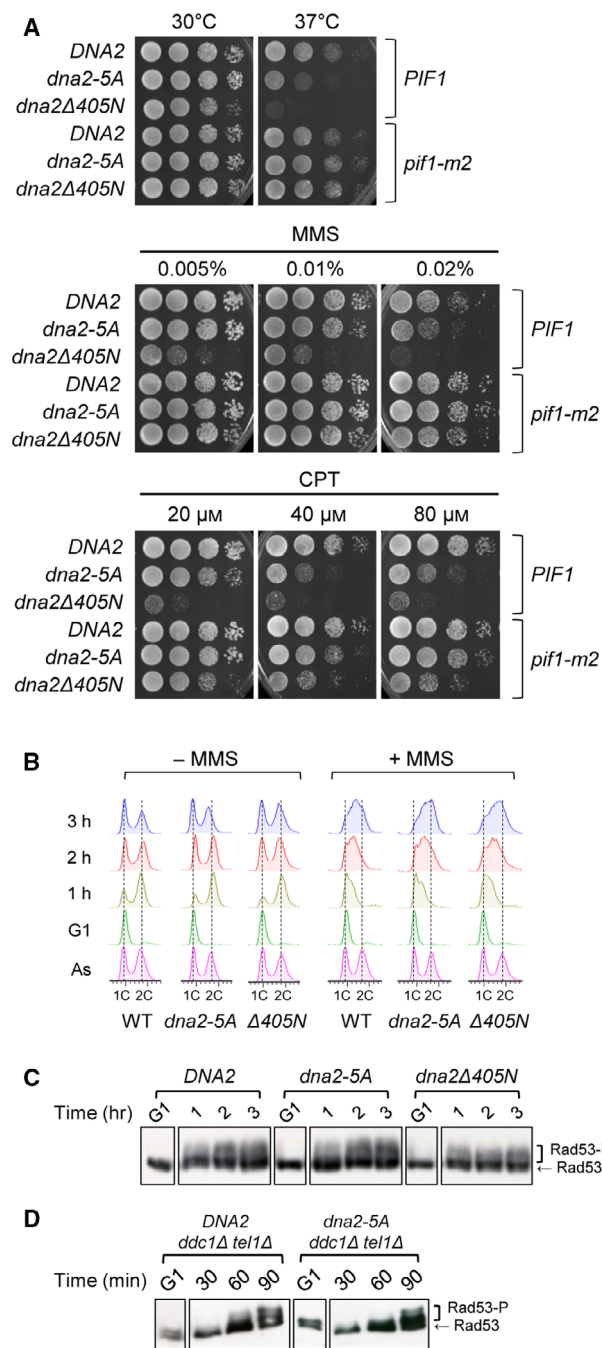


Fig. 7. The hairpin-flap-binding activity of Dna2 is required under replication stress conditions. **A**, Drug sensitivity of wild-type (DNA2), *dna2-5A*, *dna2Δ405N*, DNA2 *pif1-m2*, *dna2-5A pif1-m2*, and *dna2Δ405N pif1-m2* cells to methyl methanesulfonate (MMS) and camptothecin (CPT) was tested by drop dilution assay at 30 °C. These experiments were repeated three times, and one representative result was shown. **B**, Log-phase (As) cells of WT, *dna2-5A*, and *dna2Δ405N* ($\Delta405N$) were arrested to G1 phase by α -factor (G1) and released into the media lacking (-MMS) or containing 0.033% of MMS (+MMS). Samples withdrawn at each time point were analyzed by flow cytometry. **C** and **D**, Phosphorylation of Rad53 in wild-type, *dna2-5A*, and *dna2Δ405N* (**C**), and DNA2 *ddc1Δ tel1Δ* and *dna2-5A ddc1Δ tel1Δ* (**D**) cells in the presence of MMS. Rad53-P indicates the phosphorylated form of Rad53. The western blot experiments were repeated three times, and one representative result was shown

with generation of long flaps or long ssDNA containing secondary structures during Okazaki fragment processing and DSB repair.

In order to examine the cell cycle progression of *dna2-5A* and *dna2Δ405N* cells in response to MMS, G1-arrested cells were released into the media containing MMS, followed by cell cycle analysis by flow cytometry. In the absence of MMS, WT, *dna2-5A*, and *dna2Δ405N* ($\Delta405N$), cells showed a comparable pattern of cell cycle progression (Fig. 7B, -MMS). In the presence of MMS, however, majority of WT cells were shown to stay in S phase (Fig. 7B, +MMS). In contrast, the majority of $\Delta405N$ cells had traversed S phase and formed a 2C DNA content peak at 3 h. This agrees with the previous finding that the *dna2Δ405N* cells display partial loss of checkpoint function [18]. Importantly, the *dna2-5A* cells exhibited a similar cell cycle progression as $\Delta405N$ cells in the presence of MMS. This observation is consistent with the notion that *dna2-5A* cells may be partially defective in S-phase checkpoint activation. We examined the Rad53 phosphorylation state in the specific samples used in Fig. 7B to correlate cell cycle progression with checkpoint activation, and we found that phosphorylation levels of Rad53 in *dna2-5A* were comparable to those of wild-type cells in response to MMS (Fig. 7C). In contrast, *dna2Δ405N* cells displayed significant reduction in Rad53 phosphorylation. This result is not unexpected, since other checkpoint-initiating factors, namely Dpb11, Ddc1, and Tel1, are still intact in the mutant cells, which interferes with the detection of Dna2-induced Rad53 phosphorylation in *dna2-5A* cells [55–59]. Therefore, we examined Rad53 phosphorylation in *dna2-5A ddc1Δ tel1Δ* background in order to eliminate the checkpoint activation initiated by Ddc1/Dpb11 and Tel1 [60]. However, we found that the

ascribed to inefficient processing of long flaps, we incorporated *pif1-m2* allele, a nuclear-specific *pif1* null allele, into *dna2* mutants and tested whether *pif1-m2* can suppress the growth defects of *dna2* mutants above [54]. The *pif1-m2* allele efficiently suppressed temperature and MMS/CPT sensitivities of *dna2-5A* and *dna2Δ405N* cells (Fig. 7A), in keeping with the idea that the observed growth defects of the *dna2-5A* and *dna2Δ405N* cells arise from cellular events associated

Rad53 phosphorylation levels in *dna2-5A ddc1Δ tell1Δ* cells were slightly reduced in the presence of MMS compared with *DNA2 ddc1Δ tell1Δ* (Fig. 7D). One conceivable explanation for the slight reduction in Rad53 phosphorylation is due to the presence of a limited number of long flaps *in vivo* at the time of analysis. Thus, the difference in Rad53 phosphorylation levels may not be dramatic between *dna2-5A* and wild-type cells. One way to test this idea would be to construct a gain-of-function mutant strain that produces long flaps with an elevated frequency. For example, overexpression of Pif1 in *dna2-5A* could lead to accumulation of long flaps. This would help clarify that DNA-binding activity of Dna2 contributes to checkpoint activation.

Discussion

In this study, we examined the interplays between the N-terminal regulatory and C-terminal catalytic domains of Dna2 using biochemical and genetic approaches, in an attempt to understand their *in vivo* significance in relation to checkpoint.

We found that the hairpin flap DNA-binding activity of Dna2 residing in its N-terminal domain is well suited to target the Dna2 enzyme to various DNA replication intermediates that could arise during DNA replication and repair. In addition, we discovered that this specific DNA-binding activity of Dna2 is critical for cell growth under replication stress conditions caused by the presence of DNA-damaging agents such as MMS and CPT. We showed that dysfunctional catalytic activity of Dna2 induced Dna2-dependent checkpoint signaling since abrogation of Mec1-stimulation function of Dna2 rendered *dna2* catalytic mutants viable (Fig. 1B). This result suggests that Dna2/Mec1-mediated checkpoint is activated in *dna2* catalytic mutants, and the checkpoint, once activated, interferes with cell growth, being toxic to cell survival. The toxicity could result most likely from the colocalization of Dna2 and Mec1, leading to excess checkpoint signal that causes cell cycle arrest.

Our findings can be graphically summarized in a model as shown in Fig. 8. (i) In a normal growth of cell, the three biochemical (N-terminal DNA binding, and the C-terminal helicase and nuclease) activities of Dna2 collaborate in the removal of secondary-structured 5' flaps (Fig. 8, A) [18,19]. (ii) Under replication stress, cells cope with failure in timely processing of 5' flaps by Dna2, which results in generation of long ssDNA. This leads to the formation of RPA-coated ssDNA that recruits the Mec1-Ddc2 complex [12,61,62]. Dna2 can be localized to long 5' flaps through its interaction with RPA and/or through the

DNA-binding activity residing in its N- and C-terminal domains [16,18]. The Dna2 enzyme engaged in this complex can stimulate the kinase activity of the recruited Mec1 to activate checkpoint pathway (Fig. 8, B) [23,25]. (iii) When one of the two catalytic activities of Dna2 is dysfunctional, the stable colocalization of Mec1 and Dna2 could lead to hyperstimulation of Mec1, inducing Dna2-dependent checkpoint activation. The subsequent cell cycle arrest could contribute directly to the lethality/sickness of *dna2* catalytic mutants (Fig. 8, C). (iv) In the absence of hairpin-binding activity of Dna2, Dna2 fails to recognize and bind hairpin flaps, leading to accumulation of unprocessed 5' flaps over threshold levels, triggering cell cycle arrest at G2/M phase (Fig. 8, D). The mechanism by which the excess amount of unprocessed 5' flaps leads to cell cycle arrest will be discussed below.

While it is striking that the *dna2Δ105N* mutation completely abolishes the growth of the *dna2-WYK* (or *dna2-WYH*) mutant (Fig. 1C), it is not clear how the N-terminal DNA-binding activity of Dna2 is able to sustain cell viability when the catalytic activity (*dna2-KE* or *dna2-HA*) and the checkpoint activation (*dna2-WY-AA*) are simultaneously impaired. There are two possible explanations for these observations: (i) The loss of coordination between the N-terminal DNA-binding activity and the remaining nuclease activity hinders optimal functioning of Dna2 enzyme, leading to toxic intermediates accumulation, or (ii) the mutant cells are unable to tolerate the simultaneous loss of the two biochemical activities, namely N-terminal DNA-binding and C-terminal enzymatic activities.

The finding that Dna2^{405N} bound the HJ substrate with the greatest efficiency among various substrates raises the possibility that budding yeast Dna2 is involved in the resolution of HJ or reversed forks (Fig. 3D). Although the role of this activity is not clear at this point, it is worthwhile to mention that Dna2 has genetic interactions with several enzymes involved in HJ resolution such as Mus81-Mms4 and Yen1 [33,63]. Furthermore, Rad27, which physically interacts with Dna2, can efficiently stimulate the nuclease activity of Mus81-Mms4 complex [63,64]. A further study is required to understand the significance of the efficient binding of Dna2 to the HJ structure.

It was previously reported that growth defects of *dna2* catalytic mutants are suppressed by overexpression of *RAD27*, presumably by promoting the Rad27-dependent flap removal pathway and thus bypassing the need for Dna2 activity [64,65]. Likewise, the overexpression of *RAD27* restored the growth of *dna2-5A* cells at 37 °C (Fig. 6B). This indicates that the growth defect of *dna2-5A* cells could result from faulty

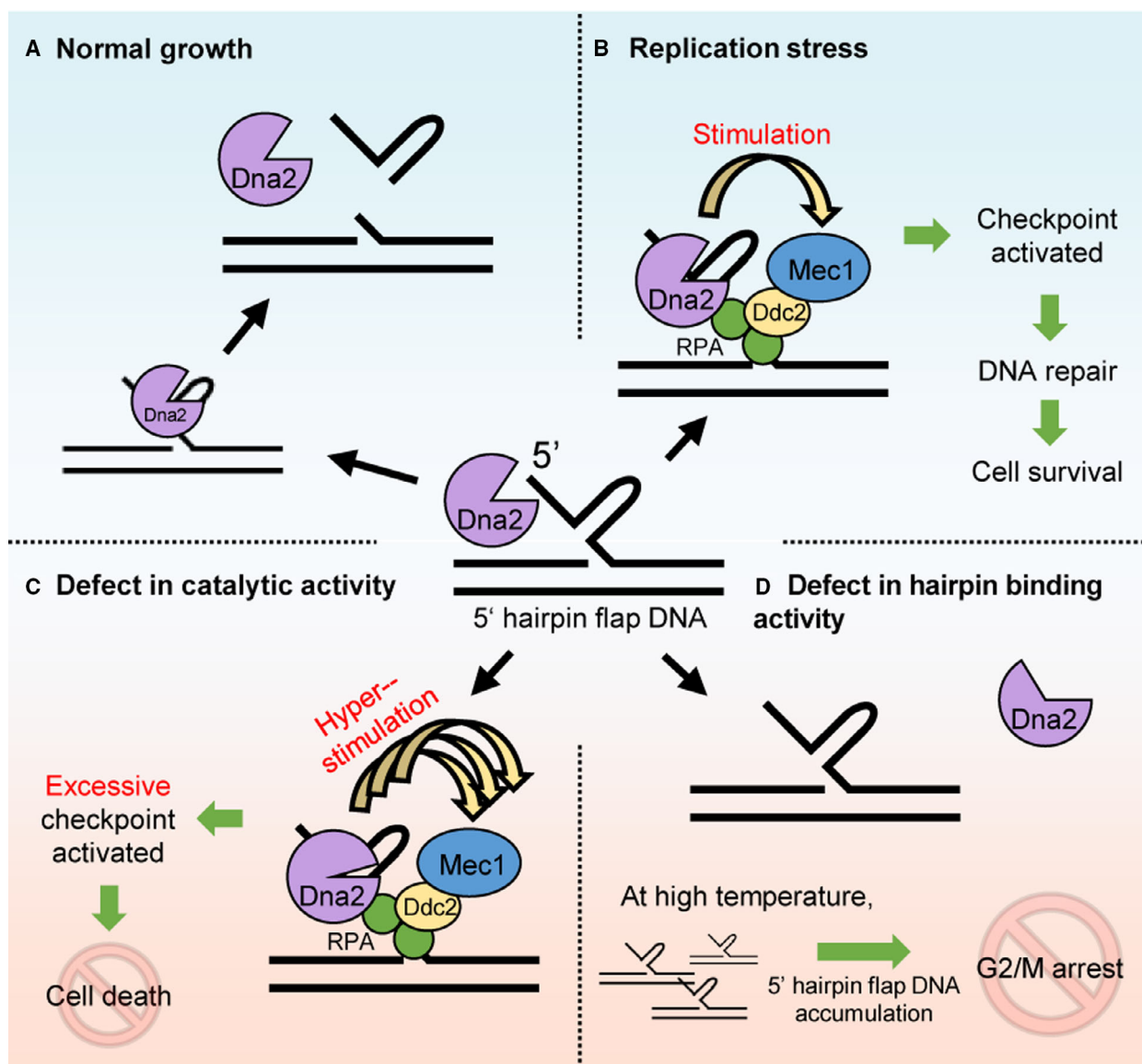


Fig. 8. A model summarizing the interplay between Dna2 and checkpoint activation. In the course of DNA replication, repair, and recombination processes, long 5' single-stranded flap DNA could develop secondary structures on their flaps. (A) These hairpin flaps can be normally processed by the coordinated action of the N-terminal DNA-binding, helicase, and nuclease activities of Dna2. (B) Inefficient processing of the flaps by Dna2 may occur under replication stress condition. The single-stranded DNA region in unprocessed flaps could then recruit RPA and Mec1-Ddc2 complex, which is subsequently stimulated by Dna2 to activate checkpoint. (C) In *dna2-KE* and *dna2-HA* cells in which catalytic activities of Dna2 are defective, the 5' hairpin flaps cannot be efficiently processed, resulting in a hyperstimulation of Mec1. The prolonged stimulation of Mec1 causes checkpoint activation, leading to cell cycle arrest. (D) In case where the hairpin DNA-binding activity of Dna2 is lost, timely processing of 5' hairpin flap is impaired. Under nonpermissive temperature condition, the accumulation of unprocessed 5' hairpin flaps results in G2/M cell cycle arrest

removal of flaps during Okazaki fragment processing. It has been shown that Dna2 is cytoplasmic during G1 phase, but is translocated to the nucleus during S phase [66]. Since Dna2 serves an essential function in the nucleus, cell growth critically depends on the level of functional Dna2 nuclease activity in the nucleus

[30,67]. For example, yeast cells harboring the *dna2-HA* allele, which retains ~ 50% of the nuclease activity of wild-type, show diminished cell viability, whereas cells harboring the nuclease-dead allele (*dna2-DA*) are completely inviable [30]. Another conceivable explanation for the faulty flap processing of the *dna2-5A*

mutation is that it disrupts the nuclear localization efficiency of the mutant Dna2-5A protein. Since *dna2-5A* cells showed robust cell growth under normal conditions (Fig. 6A and Fig. 7A), it appears that the nuclease activity and nuclear localization of Dna2-5A mutant protein are intact.

We also checked whether the *dna2-WY-AA* mutation can suppress the temperature sensitivity of *dna2-5A* cells by combining the two mutations. The result was that cells having *dna2-5A-WY-AA* allele retained temperature sensitivity to the level comparable to that of *dna2-5A* cells (data not shown). This indicates that the defective growth of *dna2-5A* cells at the elevated temperature was not caused by the Dna2-mediated checkpoint activation, unlike the *dna2* catalytic mutants. We also examined other phenotypes of *dna2-5A-WY-AA* such as sensitivity to DNA-damaging agents including MMS and CPT and found that they were also comparable to those of *dna2-5A* alone (data not shown). For this reason, we did not proceed to compare Rad53 phosphorylation and cell cycle profile of this mutant.

Our biochemical and genetic analyses suggest that the cellular defects in *dna2-5A* cells arise from inefficient targeting of the protein to secondary-structured flaps. *In vitro*, the *dna2-5A* mutation abrogated the hairpin flap DNA-binding activity of the N-terminal fragment and the full-length Dna2 proteins (Fig. 5C,D, data not shown). This suggests that the endogenous secondary-structured flaps may not be removed efficiently by the Dna2-5A protein. *In vivo*, the *pif1-m2* allele efficiently suppressed the growth defect of *dna2-5A* cells (Fig. 7A). This is in keeping with the idea that the long flaps, which may form DNA secondary structures, are likely to be the cause of the sickness of *dna2-5A* cells. In addition, the growth defect of *dna2-5A* cells at 37 °C was suppressed by the overexpression of *RFA1* (Fig. 6B). Considering that RPA functions redundantly with helicase activity of Dna2 to facilitate the removal of secondary-structured flaps [16,20], the result indicates that the growth defects of *dna2-5A* cells could be attributed largely to the unremoved secondary-structured flaps. This provides an explanation of how cell cycle arrests when unprocessed flap accumulates over threshold levels as mentioned above (Fig. 8, D).

Although we showed that the DNA-binding activity mediated by the five basic residue clusters in Dna2 could contribute to the checkpoint activation, it is not clear whether this DNA-binding activity is directly involved in the activation of S-phase checkpoint through Mec1, cell cycle progression, and cellular viability to DNA replication stress. In the previous study, it was shown that DNA was not required *in vitro* for

Dna2 to activate Mec1 [23]. This is in strong contrast to our proposal that DNA binding is important for Dna2-mediated S-phase checkpoint activation. We believe that the discrepancy could be ascribed to differences in the two systems used. *In vitro*, DNA may not have any effect on Dna2-mediated stimulation of Mec1 to phosphorylate Rad53. *In vivo*, however, binding of Dna2 to a specific DNA structure may be an essential prerequisite step to trigger the downstream event that leads to activation of Mec1, acting as an important spatial and temporal regulation. Equally possible scenario is that there could be an unknown factor *in vivo* that potentiate Dna2-mediated stimulation of Mec1 to phosphorylate Rad53 in a manner dependent on DNA lesions such as hairpin structure. This implies that Dna2 could function as a bridge between the abnormal DNA structure and checkpoint machinery.

Taken together, our results suggest that the accumulation of unprocessed 5' flaps in *dna2-5A* cells leads to G2/M cell cycle arrest at nonpermissive temperature and the regulatory activities that reside in the N-terminal domain of Dna2 become critical for cell survival under DNA replication stress condition. Our findings could shed light on the mechanism by which structure-forming repeat sequences are maintained by Dna2 during DNA replication.

Materials and Methods

Yeast strains construction

All *Saccharomyces cerevisiae* strains are derivatives of YPH499 (*MATa ura3-52 lys2-801 ade2-101 trp1-Δ63 his3-Δ200 leu2-Δ1 GAL+*). In the YJA1B strain (*dna2Δ*), wild-type *DNA2* was deleted with *HIS3*, while the viability of the strain was maintained by the plasmid, pRS316-*DNA2* [34]. The YJA2 strain (*dna2Δ405N*), devoid of the N-terminal domain (aa 1-405) of *DNA2*, was described previously [35]. The YNK01 (*dna2-5A*) strain was prepared by replacing wild-type *DNA2* gene with *dna2-5A-HIS3* by transforming with a *dna2-5A-HIS3* DNA fragment flanked by 5' (400 bp) and 3' (298 bp) untranslated regions of *DNA2*. In order to prepare *pif1-m2* mutants, genomic *PIF1* gene was replaced by transforming the *TRP1-pif1-m2* DNA fragment that has 55 bp of 5' untranslated region of *PIF1* at the N terminus. Yeast were transformed using the LiAc/SS-DNA/PEG method [68].

Oligonucleotides, chemicals, and enzymes

Oligonucleotides used for the preparation of radiolabeled substrates and ssDNA competitor were synthesized and gel-purified by Bioneer (Daejeon, Korea). [γ - 32 P]ATP

was added to a final concentration of 0.1 mM to induce protein expression, and cultures were incubated at 16 °C for 2 h. Cells were then harvested, and the following purification procedures were performed at 4 °C. The cell pellet (2.2 g) was mixed with 25 mL of T₅₀ (50 mM Tris/HCl/pH 7.8, 50 mM NaCl, 10% glycerol, 0.01% Nonidet-40, 0.5 mM PMSF, 0.5 mM benzamidine, 1 µg·mL⁻¹ leupeptin, 1 µg·mL⁻¹ pepstatin A), where the number following 'T' denotes the concentration of NaCl. Cells were then sonicated and ultracentrifuged at 66,000 × g for 30 min. The lysate (5.6 mg·mL⁻¹) was loaded onto 13 mL of T₅₀-equilibrated Q-Sepharose Fast Flow resin (GE Healthcare, Uppsala, Sweden) and subsequently washed with 20 column volumes (CVs) of T₅₀. Bound proteins were then eluted with 20 CVs of a linear salt gradient (T₅₀–T₁₀₀₀). Fractions to be pooled for the next step were chosen based on two factors: target protein levels, visualized by SDS/PAGE, and DNA-binding activity, measured by EMSA using the standard 5' hairpin flap substrate. The pooled fraction (37 mg) was dialyzed against T₁₀₀ and loaded onto a 1.5-mL Heparin Sepharose 6 Fast Flow column (GE Healthcare), pre-equilibrated with T₁₀₀. Bound proteins were eluted with 33 CVs of a linear salt gradient (T₁₀₀–T₆₀₀). The pooled fraction (2.6 mg) was adjusted to 10 mM imidazole (IDZ) and loaded onto a 1 mL Ni²⁺-nitrilotriacetic acid agarose resin (Ni-NTA; Qiagen, Hilden, Germany), pre-equilibrated with T₅₀ containing 10 mM IDZ. The resin was washed consecutively with 15 CVs of T₅₀ containing 10 mM IDZ and 5 CVs of T₅₀ containing 20 mM IDZ, followed by elution with T₅₀ containing 100 mM IDZ. The peak fraction was separated by glycerol gradient sedimentation in a Beckman SW55 Ti rotor (5 mL, 15–35% glycerol concentration in T₅₀₀) at 218,000 × g for 33 h. Fractions (200 µL) were withdrawn from the top of the gradient for analysis by SDS-PAGE and EMSA.

The N-terminal domain (aa 1-405) of Dna2 protein, tagged with GST and His₆ tags at the N terminus and C terminus, respectively, was prepared by inserting the sequence of the N-terminal domain and His₆ into the pGEX-4T1 vector and transforming it into BL21-Codon-Plus(DE3)-RIL. After the culture (0.5 L) reached an A₆₀₀ of 0.5, IPTG was added to a final concentration of 0.5 mM and cells were incubated at 37 °C for 2.5 h. After harvesting cells by centrifugation at 6000 × g for 20 min, the cell pellet (1 g) was resuspended in 20 mL of T₅₀. Subsequent purification procedures were conducted at 4 °C. The cells were sonicated and then centrifuged at 16 000 g for 30 min. IDZ was added to the supernatant (4.6 mg·mL⁻¹) to final concentration of 10 mM and loaded onto Ni-NTA resin (1 mL). After successive washes with 20 CVs of T₅₀ containing 10 mM IDZ, 20 CVs of T₅₀₀ containing 20 mM IDZ, and 20 CVs of T₅₀ containing 50 mM IDZ, proteins were eluted with T₅₀ containing 250 mM IDZ. Elution fractions that contained the target protein were selected and pooled based on the criteria stated above. The pooled fraction (0.1 mg·mL⁻¹, 0.3 mg) was

loaded onto a Glutathione Sepharose 4 Fast Flow column (1 mL; GE Healthcare) pre-equilibrated with T₁₅₀. The column was successively washed with 10 CVs of T₁₅₀, 10 CVs of T₅₀₀, and 3 CVs of T₁₅₀, followed by elution with T₁₅₀ containing 10 mM reduced L-glutathione. Truncated and point-mutated forms of GST-Dna2^{405N}-His₆ were purified similarly, except that the truncated forms were purified by Ni-NTA agarose alone.

Electrophoretic mobility shift assay

Standard reaction mixtures (20 µL) contained 50 mM Tris/HCl/pH 7.8, 2 mM DTT, 0.25 mg·mL⁻¹ BSA, 0.2 mM EDTA, 5% glycerol, 125 mM NaCl, 10 ng of poly(dI-dC), 15 fmol DNA substrate, and the indicated amount of protein. Binding mixtures were incubated at 37 °C for 10 min and subsequently loaded onto 6% polyacrylamide gels in 0.5x TBE. Protein–DNA complexes were separated at 90 V for 1 h at 4 °C. The gel was vacuum-dried and autoradiographed, and the amount of protein–DNA complex was quantified using a Typhoon FLA-7000 phosphorimager (GE Healthcare).

Subtilisin digestion of the N-terminal domain of Dna2 and LC-MS/MS

The dsDNA used in this assay was prepared by mixing 1.8 µg of pUC19 with 20 U of DpnI in a buffer containing 20 mM Tris/acetate/pH 7.9, 50 mM potassium acetate, 10 mM magnesium acetate, and 100 µg·mL⁻¹ BSA at 37 °C for 1 h in a 50 µL reaction. Dna2^{405N} (1 µg) was incubated with 180 ng of dsDNA or sscDNA (M13mp18 viral DNA) in a reaction (20 µL) containing 50 mM Tris/HCl/pH 7.8, 2 mM DTT, 0.2 mM EDTA, 5% glycerol, and 125 mM NaCl. Binding reactions were performed at 37 °C for 10 min, after which the indicated amount of subtilisin was added and reactions were further incubated at 37 °C for 10 min. The products were separated by SDS/PAGE on 15% gels and visualized by Coomassie Brilliant Blue staining.

N- and C-terminal aa sequences of the subtilisin-resistant protein fragment were identified by incubating Dna2^{405N} (4 µg) with 0.6 µg of M13mp18 in a 24 µL reaction (50 mM Tris/HCl/pH 7.8, 2 mM DTT, 0.2 mM EDTA, 5% glycerol, and 125 mM NaCl) at 37 °C for 10 min. The mixture was then incubated with subtilisin (40 ng) for 10 min at 37 °C and separated by SDS/PAGE on 15% gels. The band corresponding to the subtilisin-resistant protein fragment was excised, digested with trypsin, and subjected to LC-MS/MS (Life Science Laboratories, Seoul, Korea).

Cell cycle analysis of budding yeast

Yeast cells were grown to saturation at 30 °C in YPD (yeast extract/peptone/dextrose) medium. The cells were diluted in YPD to yield an A₆₀₀ value of 0.2 and then

grown at 30 °C until A_{600} reached 0.5. One milliliter of the culture was harvested, fixed in 70% ethanol, and stored at room temperature for 4 h (asynchronous sample). α -factor was added to the remaining culture at 15 $\mu\text{g}\cdot\text{mL}^{-1}$ to induce G1 arrest, and the culture was incubated at 30 °C for an additional 1.5 h. At this point, G1 arrest was confirmed microscopically, and an aliquot (1 mL) was withdrawn for ethanol fixation. The arrested cells were then harvested, washed, and released into fresh YPD media in the presence or absence of MMS at the designated temperature. Aliquots (1 mL) were harvested at the indicated time interval for ethanol fixation. The fixed cells were washed with 200 μL of 1x FACS buffer (200 mM Tris/HCl/pH 7.5, 20 mM EDTA), resuspended in 100 μL of RNase A solution (1 mg $\cdot\text{mL}^{-1}$ in 1x FACS buffer), and incubated at 37 °C overnight. The samples were then washed with 200 μL of 1x PBS, resuspended in 1 mL of propidium iodide solution (50 $\mu\text{g}\cdot\text{mL}^{-1}$ in 1x PBS), and stored for 2.5 h at 4 °C. Stained cells were sonicated at 30% amplitude for 10 s, diluted 10-fold in 1x PBS, and then analyzed by flow cytometry (BD LSRFortessa). A total of 30 000 events per sample were recorded for analysis.

Yeast protein extract preparation and western blotting

Protein extracts were prepared by trichloroacetic acid precipitation [31]. Western blotting was conducted as described previously [69] using an anti-Rad53 antibody (ab104232; Abcam, Cambridge, UK), diluted 1:2500.

Acknowledgements

We thank Jaehoon Kim, Chul-Hwan Lee, Young-Hoon Kang, and Buki Kwon for helpful discussions and critical reading of the manuscript. This study was funded by a grant from the National Research Foundation of Korea (2018R1A2B2004602).

Author contributions

SP and PRM performed experiments; SP, YSS, NK, and AAD designed experiments; SP and YSS analyzed data and wrote the manuscript.

Conflict of Interest

The authors declare no conflict of interest.

References

- 1 Pearson CE, Nichol Edamura K & Cleary JD (2005) Repeat instability: mechanisms of dynamic mutations. *Nat Rev Genet* **6**, 729–742.

- 2 Mirkin SM (2007) Expandable DNA repeats and human disease. *Nature* **447**, 932–940.
- 3 Orr HT & Zoghbi HY (2007) Trinucleotide repeat disorders. *Annu Rev Neurosci* **30**, 575–621.
- 4 Trinh TQ & Sinden RR (1991) Preferential DNA secondary structure mutagenesis in the lagging strand of replication in *E. coli*. *Nature* **352**, 544–547.
- 5 Kang S, Jaworski A, Ohshima K & Wells RD (1995) Expansion and deletion of CTG repeats from human disease genes are determined by the direction of replication in *E. coli*. *Nat Genet* **10**, 213–218.
- 6 Freudenreich CH, Stavenhagen JB & Zakian VA (1997) Stability of a CTG/CAG trinucleotide repeat in yeast is dependent on its orientation in the genome. *Mol Cell Biol* **17**, 2090–2098.
- 7 Richards RI & Sutherland GR (1994) Simple repeat DNA is not replicated simply. *Nat Genet* **6**, 114–116.
- 8 Kang YH, Lee CH & Seo YS (2010) Dna2 on the road to Okazaki fragment processing and genome stability in eukaryotes. *Crit Rev Biochem Mol Biol* **45**, 71–96.
- 9 Balakrishnan L & Bambara RA (2013) Okazaki fragment metabolism. *Cold Spring Harb Perspect Biol* **5**.
- 10 Bae SH, Choi E, Lee KH, Park JS, Lee SH & Seo YS (1998) Dna2 of *Saccharomyces cerevisiae* possesses a single-stranded DNA-specific endonuclease activity that is able to act on double-stranded DNA in the presence of ATP. *J Biol Chem* **273**, 26880–26890.
- 11 Liu Y, Kao HI & Bambara RA (2004) Flap endonuclease 1: a central component of DNA metabolism. *Annu Rev Biochem* **73**, 589–615.
- 12 Liu B, Hu J, Wang J & Kong D (2017) Direct visualization of RNA-DNA primer removal from Okazaki fragments provides support for flap cleavage and exonucleolytic pathways in eukaryotic cells. *J Biol Chem* **292**, 4777–4788.
- 13 Schweitzer JK & Livingston DM (1998) Expansions of CAG repeat tracts are frequent in a yeast mutant defective in Okazaki fragment maturation. *Hum Mol Genet* **7**, 69–74.
- 14 Spiro C & McMurray CT (2003) Nuclease-deficient FEN-1 blocks Rad51/BRCA1-mediated repair and causes trinucleotide repeat instability. *Mol Cell Biol* **23**, 6063–6074.
- 15 Spiro C, Pelletier R, Rolsmeier ML, Dixon MJ, Lahue RS, Gupta G, Park MS, Chen X, Mariappan SV & McMurray CT (1999) Inhibition of FEN-1 processing by DNA secondary structure at trinucleotide repeats. *Mol Cell* **4**, 1079–1085.
- 16 Bae SH, Bae KH, Kim JA & Seo YS (2001) RPA governs endonuclease switching during processing of Okazaki fragments in eukaryotes. *Nature* **412**, 456–461.
- 17 Henricksen LA, Tom S, Liu Y & Bambara RA (2000) Inhibition of flap endonuclease 1 by flap secondary structure and relevance to repeat sequence expansion. *J Biol Chem* **275**, 16420–16427.

- 18 Lee CH, Lee M, Kang HJ, Kim DH, Kang YH, Bae SH & Seo YS (2013) The N-terminal 45-kDa domain of Dna2 endonuclease/helicase targets the enzyme to secondary structure DNA. *J Biol Chem* **288**, 9468–9481.
- 19 Kao HI, Veeraghavan J, Polaczek P, Campbell JL & Bambara RA (2004) On the roles of *Saccharomyces cerevisiae* Dna2p and Flap endonuclease 1 in Okazaki fragment processing. *J Biol Chem* **279**, 15014–15024.
- 20 Bae SH, Kim DW, Kim J, Kim JH, Kim DH, Kim HD, Kang HY & Seo YS (2002) Coupling of DNA helicase and endonuclease activities of yeast Dna2 facilitates Okazaki fragment processing. *J Biol Chem* **277**, 26632–26641.
- 21 Chen X, Niu H, Chung WH, Zhu Z, Papusha A, Shim EY, Lee SE, Sung P & Ira G (2011) Cell cycle regulation of DNA double-strand break end resection by Cdk1-dependent Dna2 phosphorylation. *Nat Struct Mol Biol* **18**, 1015–1019.
- 22 Zhu Z, Chung WH, Shim EY, Lee SE & Ira G (2008) Sgs1 helicase and two nucleases Dna2 and Exo1 resect DNA double-strand break ends. *Cell* **134**, 981–994.
- 23 Kumar S & Burgers PM (2013) Lagging strand maturation factor Dna2 is a component of the replication checkpoint initiation machinery. *Genes Dev* **27**, 313–321.
- 24 Hustedt N, Gasser SM & Shimada K (2013) Replication checkpoint: tuning and coordination of replication forks in S phase. *Genes (Basel)* **4**, 388–434.
- 25 Wanrooij PH & Burgers PM (2015) Yet another job for Dna2: checkpoint activation. *DNA Repair (Amst)* **32**, 17–23.
- 26 Budd ME, Choe WC & Campbell JL (1995) DNA2 encodes a DNA helicase essential for replication of eukaryotic chromosomes. *J Biol Chem* **270**, 26766–26769.
- 27 Budd ME & Campbell JL (1995) A yeast gene required for DNA replication encodes a protein with homology to DNA helicases. *Proc Natl Acad Sci U S A* **92**, 7642–7646.
- 28 Fiorentino DF & Crabtree GR (1997) Characterization of *Saccharomyces cerevisiae* dna2 mutants suggests a role for the helicase late in S phase. *Mol Biol Cell* **8**, 2519–2537.
- 29 Formosa T & Nittis T (1999) Dna2 mutants reveal interactions with Dna polymerase alpha and Ctf4, a Pol alpha accessory factor, and show that full Dna2 helicase activity is not essential for growth. *Genetics* **151**, 1459–1470.
- 30 Lee KH, Kim DW, Bae SH, Kim JA, Ryu GH, Kwon YN, Kim KA, Koo HS & Seo YS (2000) The endonuclease activity of the yeast Dna2 enzyme is essential in vivo. *Nucleic Acids Res* **28**, 2873–2881.
- 31 Demin AA, Lee M, Lee CH & Seo YS (2017) GSK-3beta homolog Rim11 and the histone deacetylase complex Ume6-Sin3-Rpd3 are involved in replication stress response caused by defects in Dna2. *Genetics* **206**, 829–842.
- 32 Budd ME, Antoshechkin IA, Reis C, Wold BJ & Campbell JL (2011) Inviability of a DNA2 deletion mutant is due to the DNA damage checkpoint. *Cell Cycle* **10**, 1690–1698.
- 33 Olmezer G, Levikova M, Klein D, Falquet B, Fontana GA, Cejka P & Rass U (2016) Replication intermediates that escape Dna2 activity are processed by Holliday junction resolvase Yen1. *Nat Commun* **7**, 13157.
- 34 Kang YH, Kang MJ, Kim JH, Lee CH, Cho IT, Hurwitz J & Seo YS (2009) The MPH1 gene of *Saccharomyces cerevisiae* functions in Okazaki fragment processing. *J Biol Chem* **284**, 10376–10386.
- 35 Bae SH, Kim JA, Choi E, Lee KH, Kang HY, Kim HD, Kim JH, Bae KH, Cho Y, Park C & *et al.* (2001) Tripartite structure of *Saccharomyces cerevisiae* Dna2 helicase/endonuclease. *Nucleic Acids Res* **29**, 3069–3079.
- 36 Shen CK & Hearst JE (1976) Psoralen-crosslinked secondary structure map of single-stranded virus DNA. *Proc Natl Acad Sci U S A* **73**, 2649–2653.
- 37 Bae SH & Seo YS (2000) Characterization of the enzymatic properties of the yeast dna2 Helicase/endonuclease suggests a new model for Okazaki fragment processing. *J Biol Chem* **275**, 38022–38031.
- 38 Balakrishnan L, Polaczek P, Pokharel S, Campbell JL & Bambara RA (2010) Dna2 exhibits a unique strand end-dependent helicase function. *J Biol Chem* **285**, 38861–38868.
- 39 Receveur-Brechot V, Bourhis JM, Uversky VN, Canard B & Longhi S (2006) Assessing protein disorder and induced folding. *Proteins* **62**, 24–45.
- 40 Majorek KA, Porebski PJ, Dayal A, Zimmerman MD, Jablonska K, Stewart AJ, Chruszcz M & Minor W (2012) Structural and immunologic characterization of bovine, horse, and rabbit serum albumins. *Mol Immunol* **52**, 174–182.
- 41 Meszaros B, Erdos G & Dosztanyi Z (2018) IUPred2A: context-dependent prediction of protein disorder as a function of redox state and protein binding. *Nucleic Acids Res* **46**, W329–W337.
- 42 Dosztanyi Z (2018) Prediction of protein disorder based on IUPred. *Protein Sci* **27**, 331–340.
- 43 Munashingha PR, Lee CH, Kang YH, Shin YK, Nguyen TA & Seo YS (2012) The trans-autostimulatory activity of Rad27 suppresses dna2 defects in Okazaki fragment processing. *J Biol Chem* **287**, 8675–8687.
- 44 Branzei D & Foiani M (2006) The Rad53 signal transduction pathway: replication fork stabilization, DNA repair, and adaptation. *Exp Cell Res* **312**, 2654–2659.
- 45 Beranek DT (1990) Distribution of methyl and ethyl adducts following alkylation with monofunctional alkylating agents. *Mutat Res* **231**, 11–30.

- 46 Tercero JA & Diffley JF (2001) Regulation of DNA replication fork progression through damaged DNA by the Mec1/Rad53 checkpoint. *Nature* **412**, 553–557.
- 47 Hsiang YH, Hertzberg R, Hecht S & Liu LF (1985) Camptothecin induces protein-linked DNA breaks via mammalian DNA topoisomerase I. *J Biol Chem* **260**, 14873–14878.
- 48 Pommier Y (2006) Topoisomerase I inhibitors: camptothecins and beyond. *Nat Rev Cancer* **6**, 789–802.
- 49 Symington LS & Gautier J (2011) Double-strand break end resection and repair pathway choice. *Annu Rev Genet* **45**, 247–271.
- 50 Budd ME, Reis CC, Smith S, Myung K & Campbell JL (2006) Evidence suggesting that Pif1 helicase functions in DNA replication with the Dna2 helicase/nuclease and DNA polymerase delta. *Mol Cell Biol* **26**, 2490–2500.
- 51 Rossi ML, Pike JE, Wang W, Burgers PM, Campbell JL & Bambara RA (2008) Pif1 helicase directs eukaryotic Okazaki fragments toward the two-nuclease cleavage pathway for primer removal. *J Biol Chem* **283**, 27483–27493.
- 52 Pike JE, Burgers PM, Campbell JL & Bambara RA (2009) Pif1 helicase lengthens some Okazaki fragment flaps necessitating Dna2 nuclease/helicase action in the two-nuclease processing pathway. *J Biol Chem* **284**, 25170–25180.
- 53 Ryu GH, Tanaka H, Kim DH, Kim JH, Bae SH, Kwon YN, Rhee JS, MacNeill SA & Seo YS (2004) Genetic and biochemical analyses of Pfh1 DNA helicase function in fission yeast. *Nucleic Acids Res* **32**, 4205–4216.
- 54 Schulz VP & Zakian VA (1994) The saccharomyces PIF1 DNA helicase inhibits telomere elongation and de novo telomere formation. *Cell* **76**, 145–155.
- 55 Majka J, Niedziela-Majka A & Burgers PM (2006) The checkpoint clamp activates Mec1 kinase during initiation of the DNA damage checkpoint. *Mol Cell* **24**, 891–901.
- 56 Kumagai A, Lee J, Yoo HY & Dunphy WG (2006) TopBP1 activates the ATR-ATRIP complex. *Cell* **124**, 943–955.
- 57 Mordes DA, Nam EA & Cortez D (2008) Dpb11 activates the Mec1-Ddc2 complex. *Proc Natl Acad Sci U S A* **105**, 18730–18734.
- 58 Morrow DM, Tagle DA, Shiloh Y, Collins FS & Hieter P (1995) TEL1, an *S. cerevisiae* homolog of the human gene mutated in ataxia telangiectasia, is functionally related to the yeast checkpoint gene MEC1. *Cell* **82**, 831–840.
- 59 Bakkenist CJ & Kastan MB (2003) DNA damage activates ATM through intermolecular autophosphorylation and dimer dissociation. *Nature* **421**, 499–506.
- 60 Navadgi-Patil VM & Burgers PM (2009) The unstructured C-terminal tail of the 9-1-1 clamp subunit Ddc1 activates Mec1/ATR via two distinct mechanisms. *Mol Cell* **36**, 743–753.
- 61 Zou L, Liu D & Elledge SJ (2003) Replication protein A-mediated recruitment and activation of Rad17 complexes. *Proc Natl Acad Sci U S A* **100**, 13827–13832.
- 62 Rouse J & Jackson SP (2002) Lcd1p recruits Mec1p to DNA lesions in vitro and in vivo. *Mol Cell* **9**, 857–869.
- 63 Kang MJ, Lee CH, Kang YH, Cho IT, Nguyen TA & Seo YS (2010) Genetic and functional interactions between Mus81-Mms4 and Rad27. *Nucleic Acids Res* **38**, 7611–7625.
- 64 Budd ME & Campbell JL (1997) A yeast replicative helicase, Dna2 helicase, interacts with yeast FEN-1 nuclease in carrying out its essential function. *Mol Cell Biol* **17**, 2136–2142.
- 65 Lee M, Lee CH, Demin AA, Munashingha PR, Amangyeld T, Kwon B, Formosa T & Seo YS (2014) Rad52/Rad59-dependent recombination as a means to rectify faulty Okazaki fragment processing. *J Biol Chem* **289**, 15064–15079.
- 66 Kosugi S, Hasebe M, Tomita M & Yanagawa H (2009) Systematic identification of cell cycle-dependent yeast nucleocytoplasmic shuttling proteins by prediction of composite motifs. *Proc Natl Acad Sci U S A* **106**, 10171–10176.
- 67 Budd ME, Choe W & Campbell JL (2000) The nuclease activity of the yeast DNA2 protein, which is related to the RecB-like nucleases, is essential in vivo. *J Biol Chem* **275**, 16518–16529.
- 68 Gietz RD & Woods RA (2002) Transformation of yeast by lithium acetate/single-stranded carrier DNA/polyethylene glycol method. *Methods Enzymol* **350**, 87–96.
- 69 Vialard JE, Gilbert CS, Green CM & Lowndes NF (1998) The budding yeast Rad9 checkpoint protein is subjected to Mec1/Tel1-dependent hyperphosphorylation and interacts with Rad53 after DNA damage. *EMBO J* **17**, 5679–5688.